

Dislocation structures in micron-sized Ni single crystals produced via tension–compression cyclic loading

Takashi Sumigawa^{a,*}, Nobutaka Kawakatsu^b, Akihiro Tobise^b, Kota Sugisaka^a,
Yoshimasa Takahashi^c, Shigeo Arai^d, Masataka Abe^a, Hiroyuki Shima^e, Yoshitaka Umeno^f

^a Department of Energy Conversion Science, Kyoto University, Yoshida-honmachi, Sakyo-ku, Kyoto 606-8501, Japan

^b Department of Mechanical Engineering and Science, Kyoto University, Kyotodaigaku Katsura, Nishikyo-ku, Kyoto 615-8540, Japan

^c Department of Mechanical Engineering, Kansai University, 3-3-35 Yamate-cho, Suita-shi, Osaka 564-8680, Japan

^d Institute of Materials and Systems for Sustainability (IMaSS), Nagoya University, Furo-cho, Chikusa-ku, Nagoya 464-8603, Japan

^e Department of Environmental Sciences, University of Yamanashi, 4-4-37, Takeda, Kofu 400-8510, Japan

^f Institute of Industrial Science, The University of Tokyo, 4-6-1, Komaba, Meguro-ku, Tokyo 153-8505, Japan

ARTICLE INFO

Keywords:

Micron scale
Fatigue
Dislocation
Cyclic loading
Single crystal

ABSTRACT

The strength and deformation characteristics of micron-sized metals under monotonic loading have long been investigated. In contrast, despite its practical significance, their fatigue behavior remains unexplored. To this end, tension–compression fatigue tests were conducted herein on micron-sized Ni single crystals to elucidate their fatigue behavior and internal dislocation structures. Specimens with square cross sections of 5 and 2 μm on a side were prepared and subjected to cyclic loading at low stress amplitudes, which did not induce fatigue cracking in bulk metals. Remarkably, fatigue cracks were not present in 5- μm -wide specimens, whereas intrusions/extrusions were observed in 2- μm -wide specimens, leading to crack initiation. Vein-like structures comprising edge dislocations were observed in 5- μm -wide specimens, which are commonly observed in bulk metals. Conversely, the dislocation structure in 2- μm -wide specimens resembled that associated with persistent slip bands, which cause intrusions/extrusions and fatigue cracking in bulk metals under high stress amplitudes. The experimental findings indicate that the fatigue behavior of small-sized metal single crystals is characterized by the absence of vein formation.

1. Introduction

Metal fatigue is the cause of the majority of serious accidents involving industrial structures; therefore, the related mechanism has been widely studied. In particular, electron microscopes have enabled the observation of the morphology of such metals, facilitating better understanding of the relation between unique dislocation structures and surface fatigue damage [1–4]. The fundamental fatigue properties of single crystals of metals such as copper (Cu) [5–8], nickel (Ni) [9–11], and silver [12] and stainless steel [13] have been investigated. Fig. 1(a) shows a typical cyclic stress–strain curve (CSSC) obtained from fully reversed tension–compression cyclic loading tests performed on metal single crystals arranged in a single slip orientation. The vertical and horizontal axes represent the saturation-resolved shear stress amplitude and plastic shear strain amplitude, respectively. The curve can be divided into three regions, namely A, B, and C, where different fatigue

dislocation structures are formed. At low plastic shear strain amplitudes (region A), veins comprising edge dislocation dipoles and channels with low dislocation densities appear (Fig. 1(b)). As the applied strain amplitude increases, the saturation stress amplitude eventually plateaus (region B) and crystallographic slip deformations are localized within narrow bands. Within these bands, narrow walls composed of edge dislocation dipoles are periodically arranged (ladder-like dislocation structure; Fig. 1(c)). The localized deformation zone is known as the “persistent slip band (PSB)” [14–17], and the glide of screw dislocations between the dislocation walls may carry a high degree of plastic strain [18]. The saturation stress amplitude in region B provides the stress amplitude for PSB formation, $\Delta\tau_{\text{PSB}}/2$. The irreversibility of shear displacements due to crystallographic slip within the PSBs produces extrusions and intrusions on the surfaces [19–22]. As fatigue cracks are generally initiated at the root of intrusions or the interface between the PSB and matrix, the formation of PSB (ladder-like dislocation structure)

* Corresponding author.

E-mail address: sumigawa.takashi.2c@kyoto-u.ac.jp (T. Sumigawa).

<https://doi.org/10.1016/j.actamat.2024.120208>

Received 18 April 2024; Received in revised form 13 July 2024; Accepted 18 July 2024

Available online 20 July 2024

1359-6454/© 2024 The Authors. Published by Elsevier Ltd on behalf of Acta Materialia Inc. This is an open access article under the CC BY license (<http://creativecommons.org/licenses/by/4.0/>).

primarily causes fatigue fracture. In region C, the saturation stress amplitude increases again and labyrinth and cell structures are formed. The dimensions of these fatigue substructures are independent of the material size ranging from one to several micrometers [23]. Therefore, specimens with three-dimensional sizes smaller than the micrometer level are expected to possess unique fatigue behavior because conventional fatigue substructures cannot be formed.

Fully reversed fatigue tests have been performed on three-dimensional micron-sized metal single crystals. The Bauschinger effect on mechanical and microstructural properties of crystals have been studied via bending cyclic loading [24,25]. In addition, it was found that fatigue strength increases with decreasing material size [26,27]. However, as inhomogeneous strain in bending deformation (gradient strain distribution) strongly affects the plastic deformation due to dislocation pile up in the neutral plane [28], the fatigue mechanisms of micron-sized metals is desirably elucidated using uniaxial cyclic loading methods. Fully reversed tension–compression tests without strain gradients have been performed on Cu and Ni single crystals with widths of 1–10 μm [29–32]. In the 10- μm -wide Ni single crystals, higher number of cycles was required for PSB formation; however, the ladder-like dislocation structures were similar to bulk structures [31]. In contrast, in 2- μm -wide Cu single-crystals [32] with dimensions comparable to the bulk fatigue dislocation structure, the relation between the saturation stress amplitudes and plastic strain did not coincide with CSSC for bulk Cu. Moreover, extrusions/intrusions and fatigue cracks were generated at stress amplitudes lower than $\Delta\tau_{\text{PSB}}/2$ and the fatigue life was reduced. This indicates that micron-sized metal single crystals have a peculiar fatigue phenomenon; however, the fatigue dislocation structures necessary for exploring the fatigue mechanism have not been clarified.

In this study, tension–compression cyclic loading tests were performed on Ni single crystals with cross-sectional dimensions similar to those of the fatigue microstructures in the bulk metal. Then, the morphology of specimens was observed via ultra-high voltage transmission electron microscopy (UHV-TEM). The aim of this study is to examine the dislocation structures in micron-sized metal single crystals subjected to tension–compression cyclic loading at stress amplitudes lower than $\Delta\tau_{\text{PSB}}/2$ of the bulk metal.

2. Experimental

2.1. Material and specimens

Nickel was chosen as the target material. Ni single crystals arranged in a single slip orientation have a CSSC, which is divided into three regions shown in Fig. 1(a). A polycrystalline Ni plate (99.999 %) (Nilaco, Japan) was prepared and its surface was polished to mirror finish using emery paper (#100–2000) and diamond paste with particle sizes of 1

and 3 μm (Stuers, Denmark). For grain coarsening and residual strain removal, the plate was heated at 1073 K for 8 h under a high-vacuum environment (1×10^{-8} Pa, base pressure). Electron backscatter diffraction (EBSD) (NordlysNano, Oxford Instruments, England) measurements (step size: 1.5 μm , operating voltage: 25 kV, tilt angle of sample: 70° , software: AZtek HKL and HKL Channel 5) were conducted to determine the grain shapes and crystallographic orientations on the plate surface. As shown in Fig. 2(a), the grains grew to several hundred micrometers in diameter, sufficiently large to obtain multiple micron-sized specimens from a single grain. The Ni plate was placed in a focused ion beam (FIB) system (FB2200, Hitachi High-Tech, Japan) and the shape of grains on the plate surface were obtained using scanning ion microscopy (SIM) images. A grain with a desired orientation was identified by comparing the SIM image with the results of EBSD analysis (Fig. 2(a)). A block of tens of micrometers was carved out from the grain and mounted on the flat end of a brass wire via a built-in microprobe and tungsten (W) vapor deposition. Then, micron-sized metal single crystals were fabricated in a dog-bone shape using the FIB (accelerating voltage: 40 kV; current: 0.1–10 nA). After fabrication, the specimens were confirmed to be single crystals by SIM images. The FIB processing introduces the damaged layer with a thickness of several tens of nanometers on the specimen surface. As this layer could considerably affect the mechanical properties of the samples, low-acceleration-voltage argon ion milling (Gentle mill-hi, Hitachi High-tech, Japan) (accelerating voltage: 0.3 kV; current: 8 μA ; processing time: 25–40 min. per side) was performed to remove the layer before subsequent testing.

Fig. 2(b) illustrates the test specimen morphology. The micron-sized Ni single crystals comprise a top part, a gauge part (with a square cross-section), and a base part. Curvature was provided at the corners between the base and gauge parts and between the top and gauge parts to relieve stress concentrations. After preliminary trial and error, the height and width aspect ratio of the gauge part was set to approximately 3 to prevent buckling during compression. The four side surfaces were designated as “front surface”, “left surface”, “right surface”, and “back surface”. Six specimens were prepared in total: three with a gauge part width of 2 μm (specimens 2–1–2–3) and three with a width of 5 μm (specimens 5–1–5–3). Fig. 2(c) shows the field emission scanning electron microscopy (FE-SEM) images of the gauge parts of specimens 2–1 and 5–1. Ni, a face-centered cubic metal, has three slip directions on each of its four slip planes for a total of 12 crystallographic slip systems. In the stereograph shown in Fig. 2(d), the slip planes are labeled A–D and the slip directions are labeled 1–6, based on the Schmid and Boas notation. Using this notation, the primary slip system is labeled as B4. Fig. 2(e) shows the Schmid factors for the 12 slip systems and indicates that the B4 system has the largest value of 0.48. This indicates that the specimens are orientated so that only slip system B4 is preferentially active among the 12 slip systems (single slip orientation). Fig. 2(f)

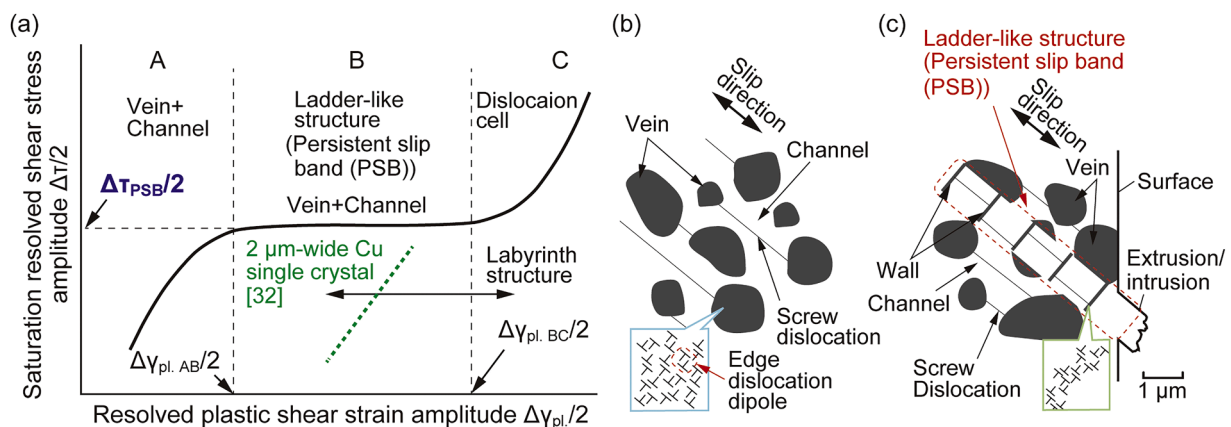


Fig. 1. (a) Typical cyclic stress-strain curve (CSSC) obtained from metal single crystals (bulk) arranged to a single slip orientation, (c) vein and channel structure, and (b) ladder-like structure of persistent slip band (PSB).

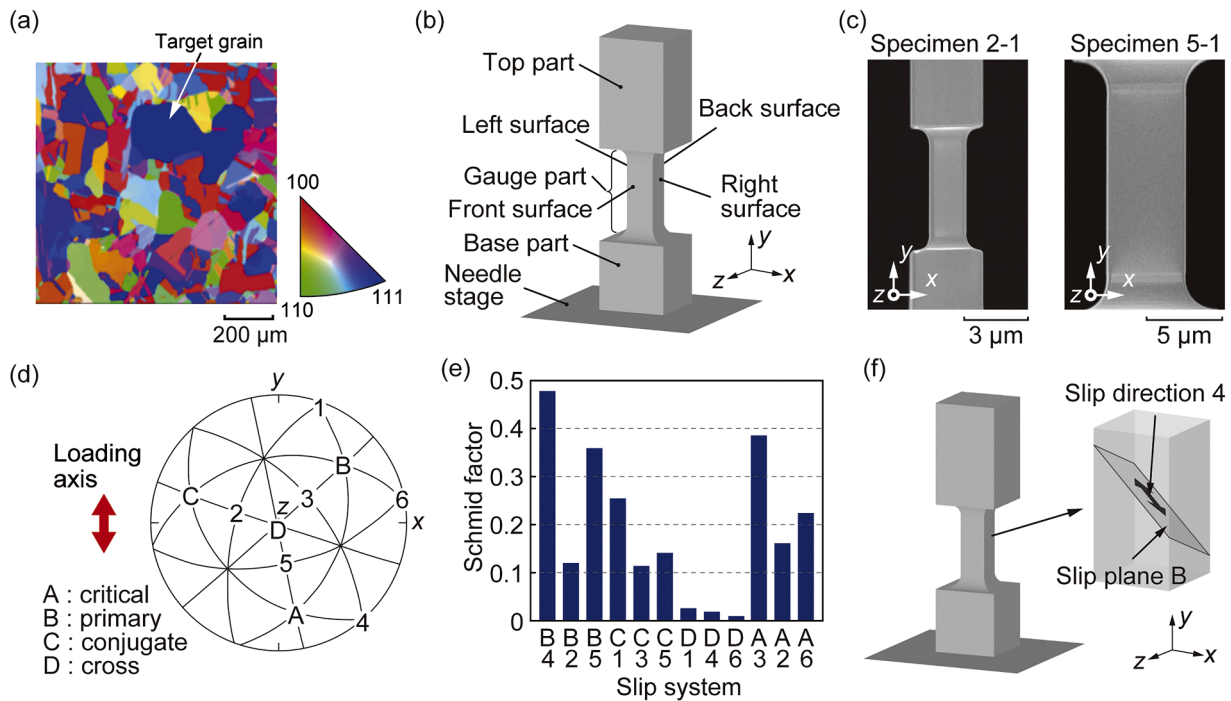


Fig. 2. (a) Inverse pole figure map of Ni polycrystalline plate after thermal treatment, (b) schematic and definition of the four sides of the gauge part of micron-sized specimen, (c) FE-SEM images of specimens, (d) stereographic projection with slip planes and slip directions based on the Schmid and Boas notation, (e) Schmid factors of 12 slip systems, and (f) schematic of the primary slip system in the specimen.

illustrates the primary slip plane B and direction 4 in the gauge part. The primary slip direction 4 is parallel to the front surface.

2.2. Testing method and condition

Tension–compression fatigue tests were performed using a loading device for micron-sized samples (Unisoku, Japan) [30]. The apparatus comprises a piezoelectric actuator, a load cell with a capacity of 500 mN, a capacitive displacement sensor, and a gripper. The device can apply cyclic displacements under a constant amplitude to the specimen. The load and displacement values resolutions are 1 μN and 0.6 nm, respectively. The load cell and displacement sensor were calibrated before the tests. Two hundreds points of load and displacement data are acquired per cycle and imported into a control PC.

The specimens were first oriented precisely to the gripper and left standing for at least 12 h to eliminate any system drift effects. The gripper could be opened and closed symmetrically relative to the central axis and could grip or release one end of the specimen using a built-in microactuator (Fig. 3(a)). As the dislocations generated at the location where mechanical gripping was performed might flow into the gauge part, the specimen was gripped near the tip of the top part. Fig. 3(b)

shows a TEM image of the gauge part of an extra specimen with a 5 μm -width after gripping, which was thinned to 200 nm using FIB processing. The black areas outside both sides of the specimens were protective tungsten films. No dislocation inflow from the top part was observed; however, a few initial dislocations existed in the gauge part. The dislocation density obtained using a stereological method [33] was calculated from images as $\sim 5.9 \times 10^{12}/\text{m}^2$, close to dislocation density of well-annealed metals ($10^{10}/\text{m}^2$ – $10^{12}/\text{m}^2$). The entire loading device was installed inside an FE-SEM (SU5000, Hitachi Hi-Tech, Japan) for detailed *in-situ* observations of the fatigue process. Tension–compression cyclic deformation tests were performed at a constant displacement amplitude. The applied displacement amplitude, $\Delta\delta/2$, was chosen to obtain saturation-resolved shear stress amplitudes in the primary slip system B4, which was lower than $\Delta\tau_{\text{PSB}}/2$ (~ 52 MPa for Ni single crystals¹²). Sinusoidal deformation was applied to each specimen at a frequency of 1 Hz with a displacement ratio, $\delta_{\text{min}}/\delta_{\text{max}} = -1$, while recording the load, and displacement at 0.005 s intervals. Table 1 summarizes the specimens, the applied number of cycles and applied displacement amplitude, $\Delta\delta/2$. Note that $\Delta\delta/2$ includes the displacement of the strain generator of the load cell. For specimens 2–1, 2–3, 5–1, and 5–2, cyclic loads were applied up to 3500 cycles. On the other hand, for

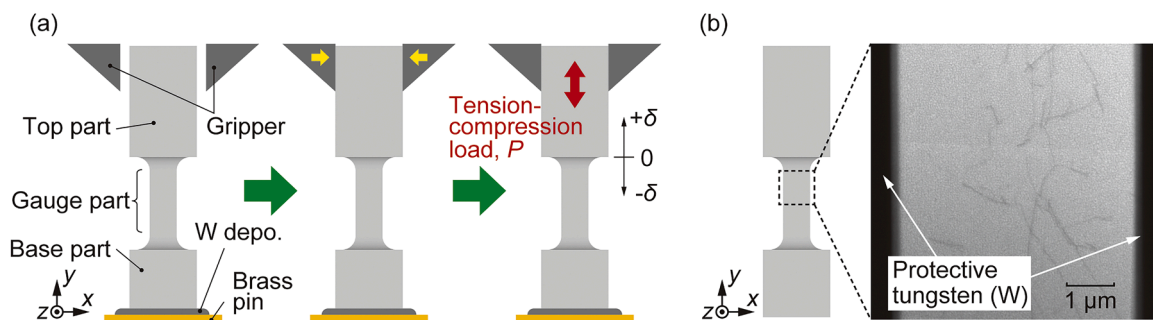


Fig. 3. (a) Specimen gripping for uniaxial tension–compression loading, and (b) TEM image of gauge part after gripping.

Table 1

Applied displacement amplitudes, number of cycles applied to each specimen and average amplitudes after saturation.

Specimen	$\Delta\delta/2$	N	$\Delta\tau_{\text{sat}}/2$	Specimen	$\Delta\delta/2$	N	$\Delta\tau_{\text{sat}}/2$
specimen 2-1	100 nm	3500	36.4 MPa	specimen 5-1	525 nm	3500	33.9 MPa
specimen 2-2	100 nm	15,000	40.4 MPa	specimen 5-2	575 nm	3500	38.3 MPa
specimen 2-3	100 nm	3500	42.9 MPa	specimen 5-3	525 nm	30,000	36.9 MPa

specimens 2-2 and 5-3, cyclic loads were applied up to 15,000 and 30,000 cycles, respectively, in order to confirm whether there were no noticeable changes after 3500 cycles.

After each test, the specimen surfaces were carefully observed using a high-resolution FE-SEM (S-5500, Hitachi Hi-Tech, Japan). Then, the specimens were thinned to approximately 200 nm via FIB processing, and the damaged layer was removed via Ar ion milling. Subsequently, their interior structures were examined via UHV-TEM (JEM-1000 K RS, JEOL, Japan). Tungsten was deposited on the specimen using the FIB apparatus to enhance their rigidity and suppress warpage during thinning. *In situ* SEM observations were performed in vacuum ($< 2.0 \times 10^{-3}$ Pa) at an accelerating voltage of 3.0 kV. The cyclic loading tests were interrupted at specific cycles to acquire high-resolution FE-SEM images at a low scan speed.

3. Results and discussion

3.1. Load-displacement curves

Fig. 4 shows typical load-displacement curves up to $N = 50$. The vertical axis represents the deviation from the average load in each cycle. For specimen 5-2 (Fig. 4(a)), a plastic strain displacement amplitude $\Delta\delta_{\text{pl}}/2$ was observed at $N = 1$, which decreased with

increasing number of cycles. This indicated work-hardening. On the other hand, specimen 2-1 (Fig. 4(b)) did not show significant decrease in $\Delta\delta_{\text{pl}}/2$. Similar behavior was observed for the other specimens.

3.2. Variations in displacement and stress amplitudes

Fig. 5 shows the plots of (a) displacement amplitude, $\Delta\delta/2$, and (b) resolved shear stress on the primary slip system B4, $\Delta\tau_{\text{B4}}/2$, as a function of the number of cycles, N , for specimens. The resolved shear stress can be obtained by

$$\tau_{\text{rss}} = P/A \cdot m, \quad (1)$$

where A is the cross-sectional area of the gauge part and m is the Schmid factor. As shown in Fig. 5(a), the displacement amplitudes remained a constant throughout the tests. In Fig. 5(b), the stress amplitudes of the 5- μm -wide specimens increased during the first few tens of cycles. However, the stress amplitude of each specimen remained nearly constant throughout the tests, and no significant fatigue-induced hardening or softening was observed except in the early stages. Table 1 summarizes the average amplitudes for the four specimens after saturation. Although the saturated stress amplitudes varied slightly among the specimens in the range of 34–43 MPa, they never exceeded 52 MPa, i.e., $\Delta\tau_{\text{PSB}}/2$ in

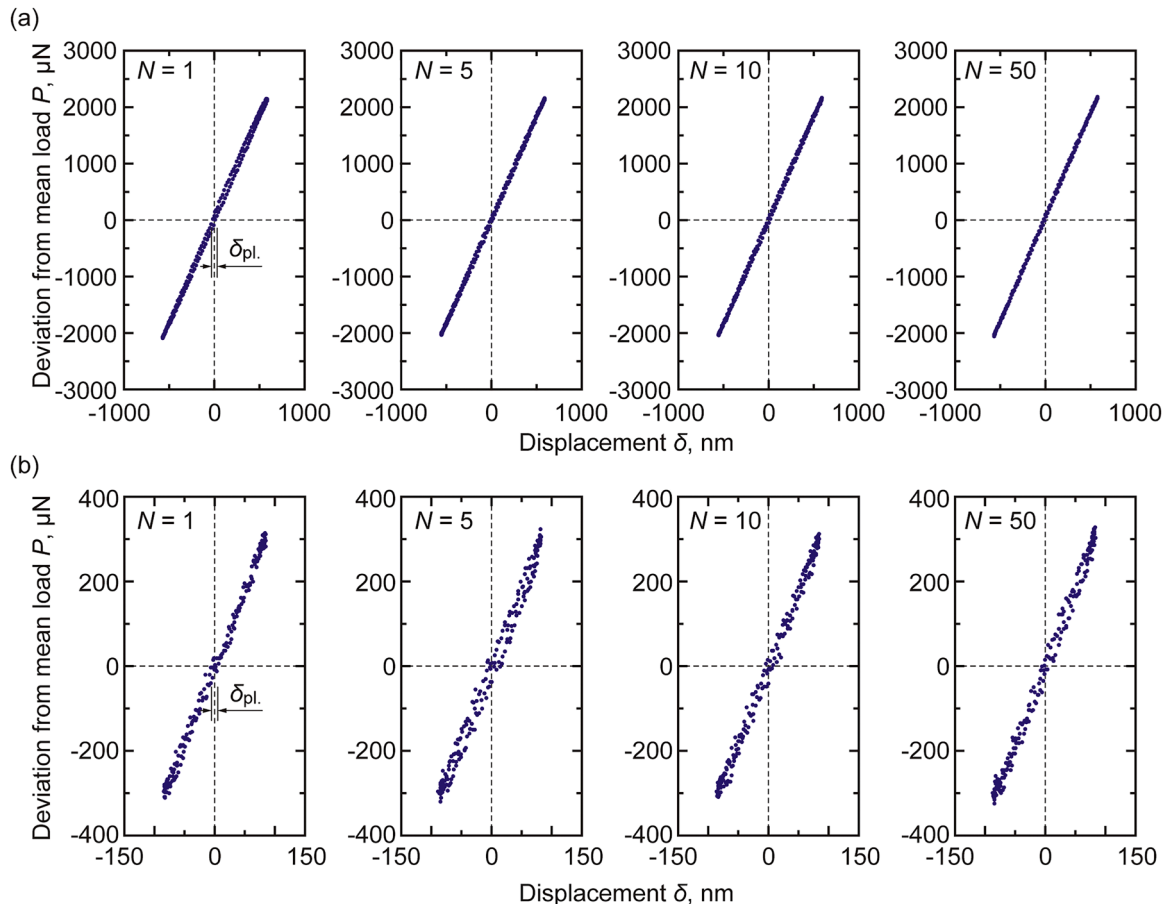


Fig. 4. Load-displacement curves at $N = 1$, $N = 5$, $N = 10$ and $N = 50$: (a) 5- μm -wide specimen (specimen 5-2) and (b) 2- μm -wide specimen (specimen 2-1).

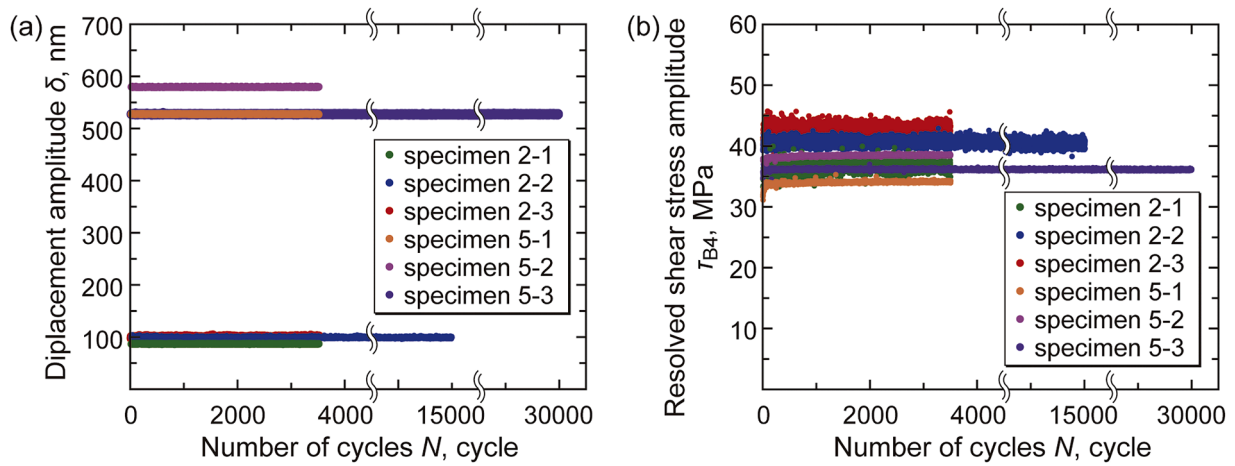


Fig. 5. Change of (a) displacement amplitude and (b) resolved shear stress amplitude during tension-compression cyclic loading tests.

the bulk Ni.

3.3. In-situ observations during testing

Fig. 6(a) shows the *in-situ* FE-SEM images for specimen 5-1. No noticeable slip zones or significant changes were evident at $N = 1$. However, the images for $N = 10$ and $N = 100$ show small waves due to a slip activity, as observed on the sides of the gauge part (i.e., left and right surfaces). Although the degree of waviness increased slightly as the number of cycles increased, it did not grow into a bump that would result in crack initiation. In specimen 5-3, where the number of cycles

was 30,000, no cracks were observed as well.

Fig. 6(b) shows the *in-situ* FE-SEM images of specimen-2-1. At $N = 1$ and $N = 10$, no evident slippage was noticed. However, at $N = 300$, slight unevenness due to slip deformation could be observed on the left and right surfaces, which developed further as the number of cycles increased. At $N = 3500$, prominent extrusions and crack-like intrusions became apparent. The process of fatigue damage in this specimen was similar to that in 2- μ m-wide single-crystal Cu specimens at resolved shear stress amplitudes lower than $\Delta\tau_{PSB}/2$ for the bulk [30,32].

Fig. 7(a) shows the SEM images of front and right surfaces of specimen 5-1 after the tension-compression test. The specimen exhibited

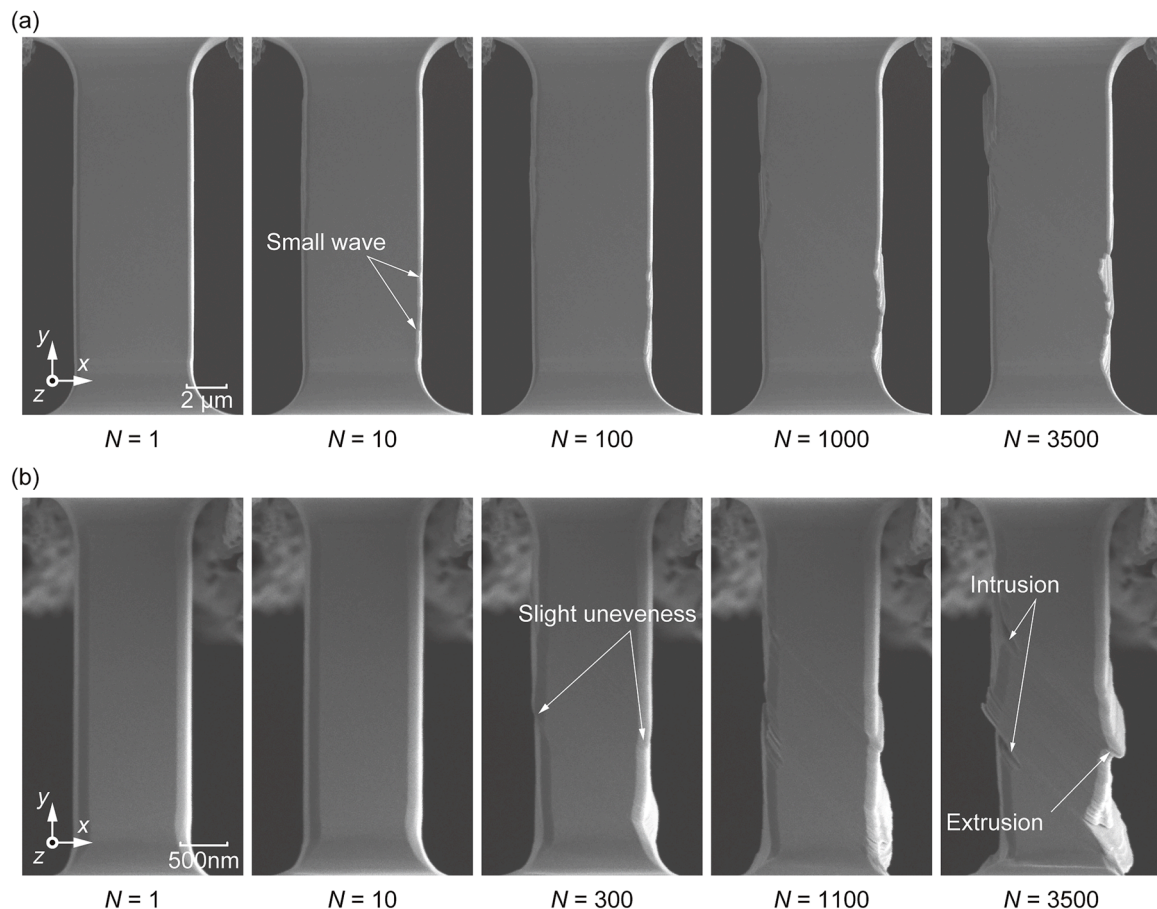


Fig. 6. (a) *In-situ* FE-SEM observation images of 5- μ m-wide specimen (specimen-5-1) and (b) 2- μ m-wide specimen (specimen-2-1).

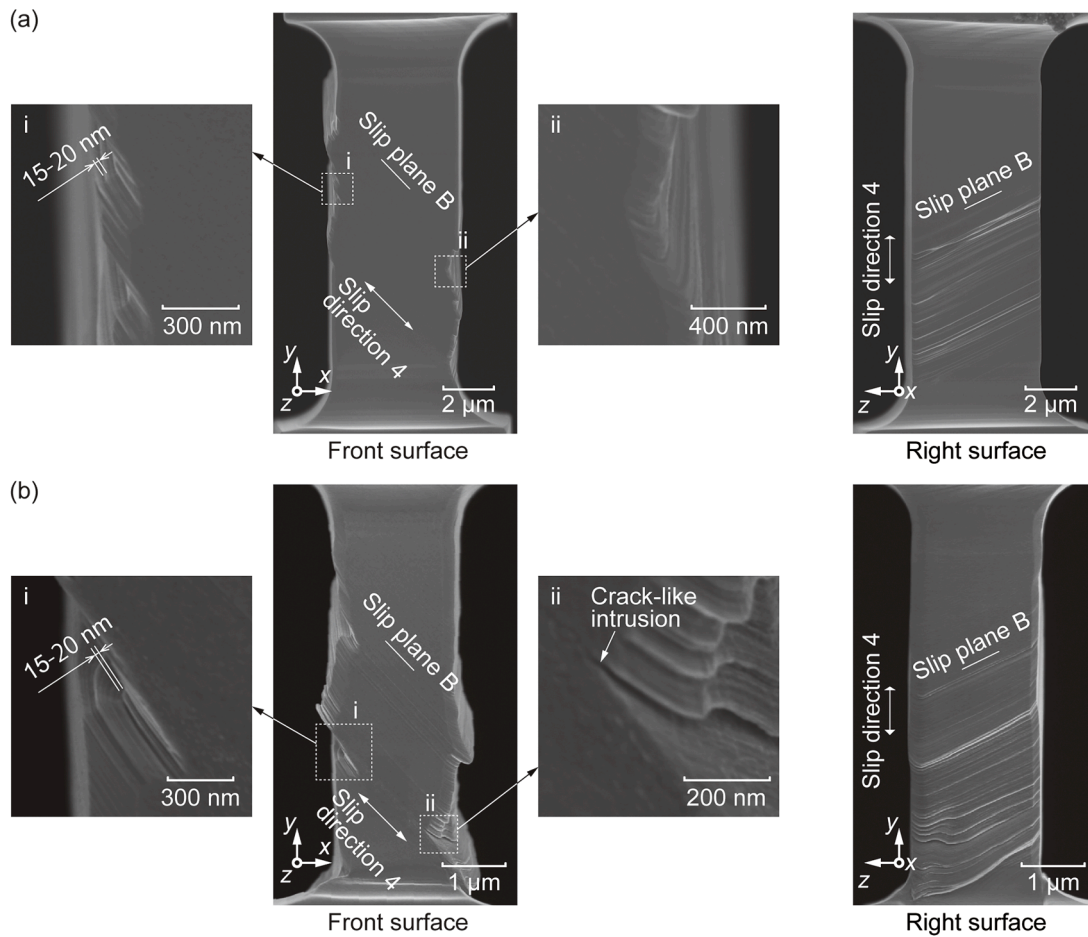


Fig. 7. FE-SEM images of the front and right surfaces of (a) specimen 5-1 and (b) specimen 2-1 after testing.

sliding at the gauge part due to the activity of the primary slip system B4, as confirmed based on the observed slip lines and slip direction. Fig. 7 (a)-i and -ii show the magnified images of the regions in which slip lines can be clearly observed. In the specimen, the slip deformation was caused by the sliding of multiple plates with thicknesses of ~15–20 nm (Fig. 7(a)-i). Small undulations can be observed on the left and right surfaces; however, these evidently did not develop into intrusions/extrusions and no cracks are visible. Other specimens (specimens 5-2 and

5-3) showed similar morphologies.

Fig. 7(b) shows the SEM images of specimen 2-1 after testing, where slip deformation due to the activity of slip system B4 can be observed. Slippage caused intrusion/extrusion to appear on the left and right surfaces of the specimen. Fig. 7(b)-i shows a magnified image of the area where this slip occurred. The deformation was caused by slippage along the slip system B4 at intervals of 15 to 20 nm. The radius of curvature at the root of the intrusion shown in Fig. 7(b)-ii was extremely small, so

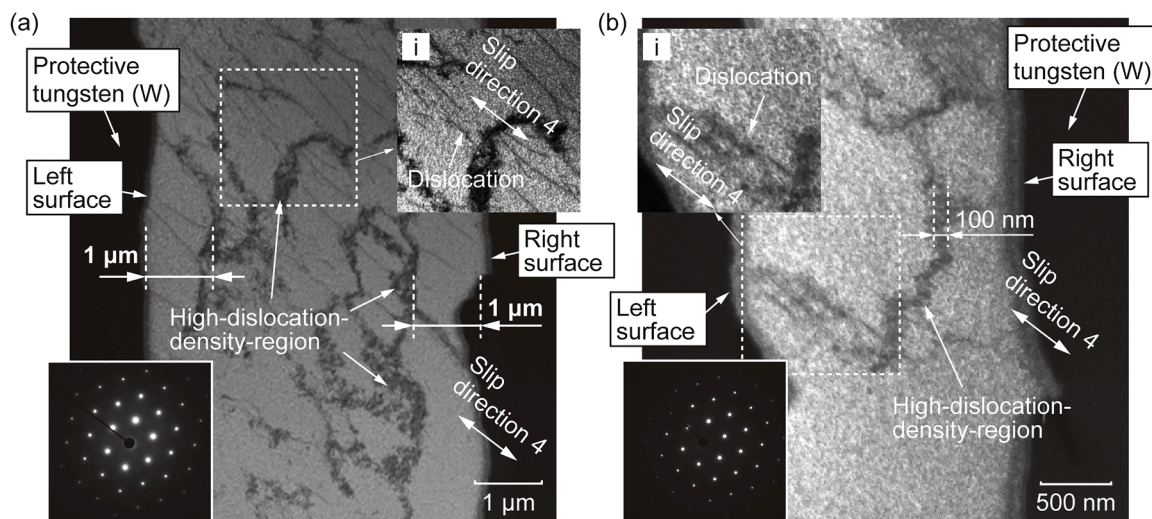


Fig. 8. STEM images of (a) specimen 5-1 and (b) specimen 2-1 after fatigue testing.

this intrusion is expected to grow into a crack. Specimens 2–2 and 2–3 also exhibited eminent extrusion and crack-like intrusion initiation.

3.4. Dislocation structures

Fig. 8(a) and (b) show the scanning transmission electron microscopy (STEM) bright-field images of the gauge parts of specimens 5–1 and 2–1, respectively. Compared with the TEM image before the test (Fig. 3(b)), the STEM images show several dislocations and a dislocation structure formed during cyclic loading. The image of specimen 5–1 (Fig. 8(a)) shows unevenly distributed regions with high-dislocation-density; dislocations parallel to the slip direction appeared (Fig. 8(a)-i), similar to the veins and channels observed in the bulk. In the case of specimen-2–1 (Fig. 8(b)), a wall-like narrow (~100-nm wide) high-dislocation-density region was observed in the middle of the gauge part, whereas no region speckled with a high density of dislocations was observed as the case for specimen-5–1 after testing. The narrow region was almost perpendicular to the slip direction, and dislocations parallel to the slip direction is visible (Fig. 8(b)-i).

To identify the properties of dislocation structures, $g\cdot b$ analyses (Appendix) were performed on 5- μm - and 2- μm -wide specimens. Fig. 9 shows (a) the STEM bright-field images taken from the [111] zone direction and (b) the dark-field images used for the $g\cdot b$ analysis of the gauge part of specimen 5–2. As shown in Fig. 9(a), high-dislocation-density regions were distributed sparsely and dislocations parallel to the primary slip direction were observed between the regions (see the enlarged view). Although these dislocations were visible in the dark-field images in Fig. 9(b)-i and ii, they mostly disappeared in Fig. 9(b)-iii. The direction where dislocations were invisible under the excitation conditions used to obtain Fig. 9(b)-iii was only $\pm 1/2[01\bar{1}]$, corresponding to the primary slip direction 4. Fig. 10(a) shows a pair of bright-field stereo images of specimen 5–2 acquired from different observation angles for the high-dislocation-density region. The high-dislocation-density-region in the left image taken from the thickness direction ([111] zone direction) of the thin specimen was thinner than that in the right image taken from the tilted direction ([114] zone direction) (see arrows in the figures). These images confirmed that the high-dislocation-density regions elongated in the thickness direction of

the thinned specimen. These results indicate that the high-dislocation-density regions comprise bundles of edge dislocations with Burgers vectors parallel to the primary slip direction 4, which is equivalent to those of veins. In addition, screw dislocations extended in the primary slip direction, as evidenced from the direction of the dislocation line and Burgers vectors. Thus, 5 μm -wide specimens developed a dislocation structure comprising veins and channels (Fig. 1(b)), equivalent to that in the bulk metal subjected to cyclic loading at a stress amplitude lower than $\Delta\tau_{\text{PSB}}/2$ in bulk Ni.

Fig. 11 shows the (a) bright-field and (b) dark-field images used for the $g\cdot b$ analysis of the gauge part of specimen 2–2, respectively. In Fig. 11(a), a narrow high-dislocation-density region with a width of several hundred nm was found in the center of the gauge part and dislocations parallel to the primary slip direction were distributed in other areas (see the enlarged view). Although these same dislocations can be observed in Fig. 11(b)-i and -ii, they are completely absent in Fig. 11(b)-iii. The excitation condition used to produce the image in Fig. 11(b)-iii make the dislocations with Burgers vectors parallel to the primary slip direction 4 invisible. Fig. 10(b) shows a pair of bright-field stereo images of specimen-2–2 acquired from different observation angles. The narrow high-dislocation-density-region in the left image ($g = 0\ 2\ \bar{2}$) becomes wider in the right image taken from the tilted direction ([121] zone direction) (see arrows in the figures). This indicates that the narrow high-dislocation-density regions have the appearance of walls standing in the thickness direction of the thinned specimen. These findings suggest that the narrow high-dislocation-density regions were dislocation walls composed of edge dislocations with Burgers vectors in the primary slip direction 4. In addition, dislocations extending in the primary slip direction constitute screw dislocations, and the regions are equivalent to the channels that are found in the bulk. Thus, the dislocation structure of 2 μm -wide specimen was similar to the ladder-like dislocation structure composed of walls and channels (Fig. 1(c)), which is seen in the bulk metal.

3.5. Fatigue of micron-sized Ni single crystal

In this study, cyclic loading tests were performed on 5- μm -wide and 2- μm -wide specimens at stress amplitudes lower than $\Delta\tau_{\text{PSB}}/2$ in the

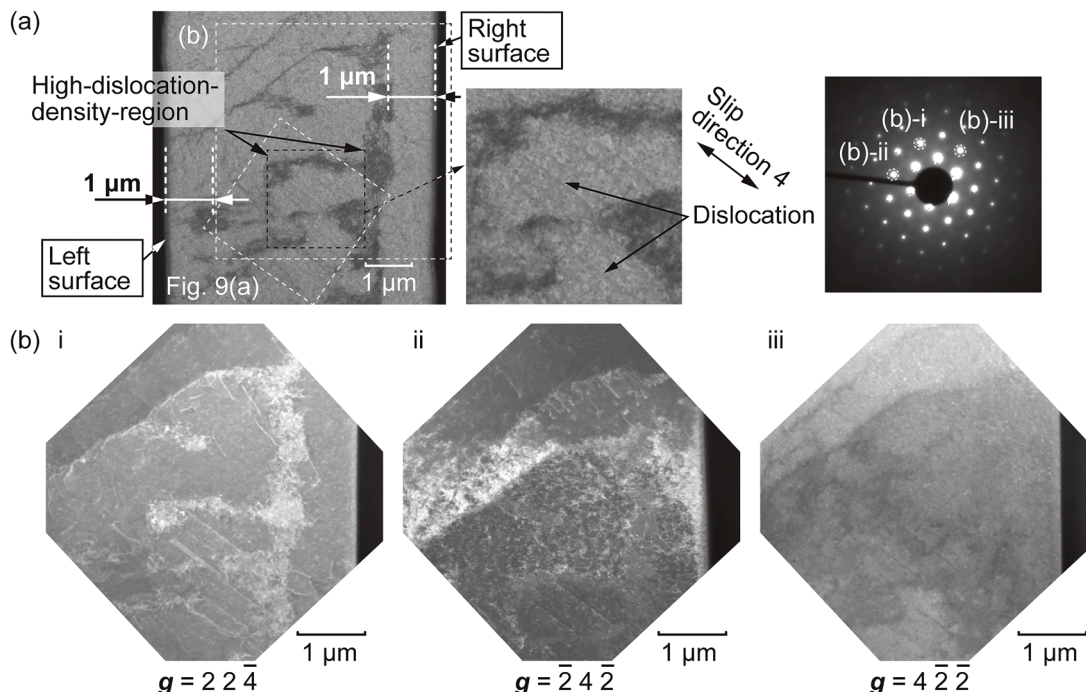


Fig. 9. (a) Bright-field images of the gauge part of specimen 5–2 and (b) dark field images for $g\cdot b$ analysis.

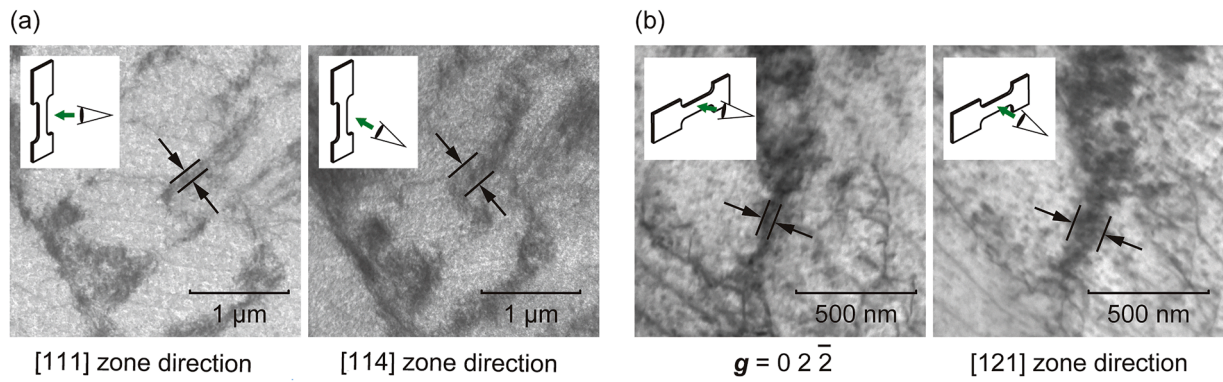


Fig. 10. Pairs of bright-field stereo images of (a) specimen-5-2 and (b) specimen-2-2.

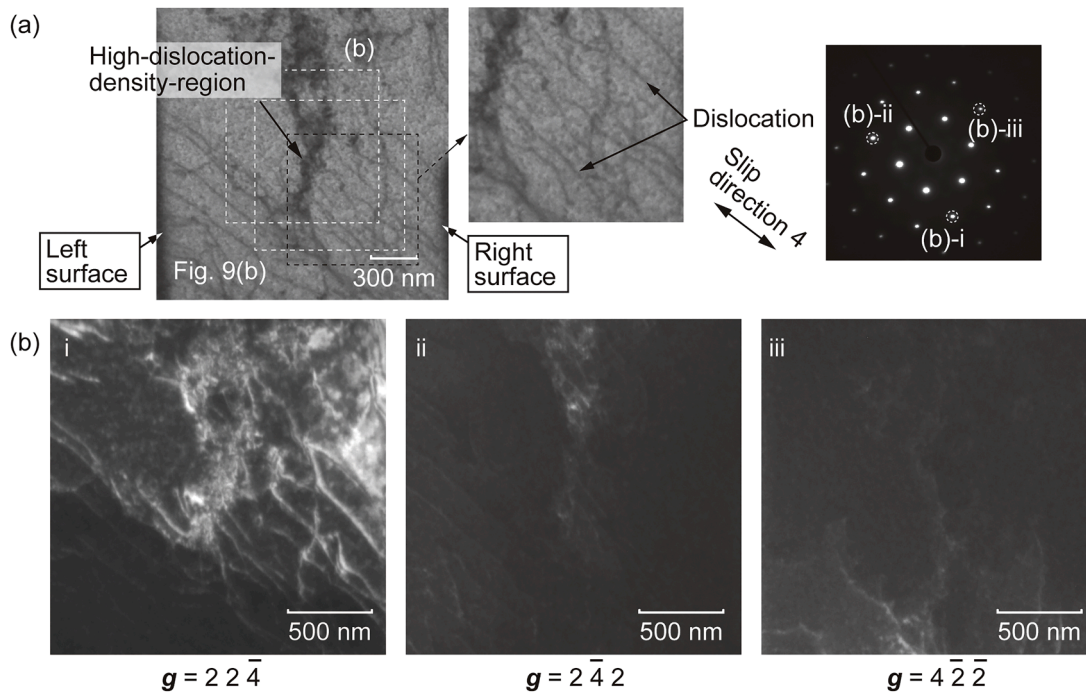


Fig. 11. (a) Bright-field images of the gauge part of specimen 2-2 and (b) dark field images for $g\cdot b$ analysis.

bulk Ni. The results revealed that only the 2- μ -wide specimens developed eminent extrusion and crack-like intrusion. This indicates that “smaller is weaker”. Detailed observation of the internal structure to identify this mechanism revealed that only 5- μ -wide specimens had a dislocation structure characterized by veins and channels, equivalent to

that in the bulk metal. The formation of the stable veins prevented fatigue cracking in specimens of this size. However, veins were conspicuously absent within approximately 1 μ m of right and left surfaces (Figs. 8(a) and 9(a)) due to the presence of an image force which is a virtual force acting on dislocations to fulfill the equilibrium equations of

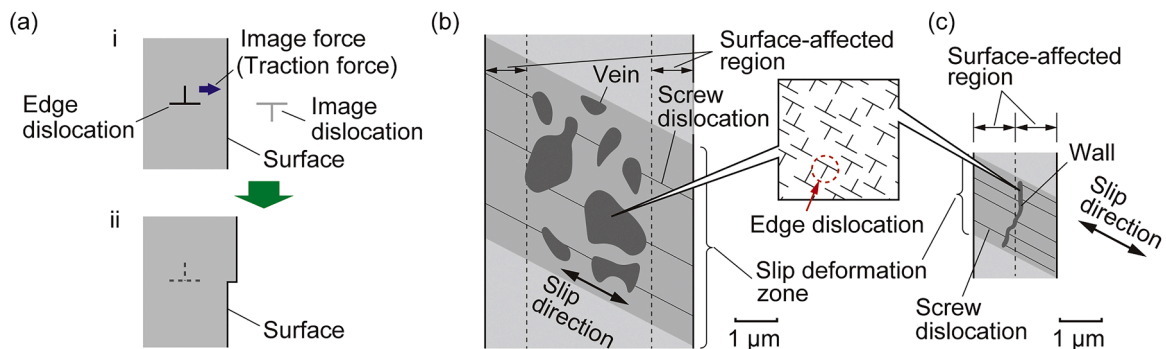


Fig. 12. (a) Schematic illustrations showing ejection of an edge dislocation from a surface by image force. Fatigue dislocation structures of (b) 5 μ m-wide and (c) 2 μ m-wide specimens after tension-compression cyclic loading.

stress at the surface [34,35] (Fig. 12(a)-i). This force considerably influenced the dislocations positioned near the surface, thereby facilitating the migration of edge dislocations with the Burgers vector in slip direction 4 positioned near the left and right surfaces and ultimately leading to their expulsion (Fig. 12(a)-ii). Consequently, in 5- μm -wide specimens, veins comprising edge dislocations failed to extend to a depth of 1 μm from the surfaces (Fig. 12(b)). The underlying rationale governing the 1- μm extent of the surface-affected region will be further investigated from a mechanical and crystallographic standpoint in the future work. On the other hand, for the 2- μm -wide specimens, this surface-affected regions of 1 μm occupied the entire gauge part (Fig. 12(c)). Therefore, veins did not develop in this specimen. Instead of thick veins, a thin dislocation wall emerged in the central region of the gauge part and screw dislocations extended on both sides of the wall, carrying plastic deformation (Fig. 12(c)). These dislocations resembled a ladder-like structure observed in the bulk metal. The PSBs, attributable to the formation of the ladder-like structure, carry significant plastic strain, thereby precipitating surface intrusions/extrusions and subsequently undergoing fatigue cracking. Based on a similar mechanism, the 2- μm -wide specimens generated intrusions/extrusions and cracks even at the stress amplitudes lower than $\Delta\tau_{\text{PSB}}/2$ in the bulk Ni. Another simulation study [36] indicated that veins changed to walls influenced by the surfaces in micron-sized metals, which complements the aforementioned mechanism. Self-organization is the result of the arrangement of dislocations into energetically lower structures owing to mechanical cyclic loading. In bulk metals subjected to cyclic loading at stress amplitudes lower than the $\Delta\tau_{\text{PSB}}/2$, the formation of veins reduces the total energy of the system. On the other hand, in environments where the material dimensions were small and the ratio of the surface-affected region (region affected by mirror forces) to volume was large, the dislocation wall with narrow widths (around 100 nm) became low-energy structures. In other words, in order to form veins, the material must have sufficient dimensions to allow for their presence. For materials containing voids or other defects inside, the fatigue strength increases with miniaturization [37]. However, in a situation where the strength is governed by the self-organized dislocation structures, such as veins and ladder-like structures, a reduction in fatigue strength due to dimensional shrinkage can occur.

Material strength augmentation via miniaturization has garnered some attention due to its potential utility in strength-oriented designs. However, the demonstrated reduction in fatigue strength of metal single crystals may raise concerns in strength design, necessitating the development of countermeasures.

4. Conclusion

The fatigue dislocation structure of Ni single crystals, featuring dimensions on the order of several micrometers, was meticulously examined and its characteristics were elucidated. Cyclic

tension–compression tests were performed on Ni single-crystals with gauge widths of 2 and 5 μm at stress amplitudes lower than the threshold for fatigue crack initiation in the bulk metal. Small undulations were generated on the surfaces of 5- μm -wide specimens; however, no intrusions/extrusions and cracks were observed and veins and channels were formed in their interiors. This fatigue behavior and microstructure were similar to those of the bulk metal. Notably, these specimens revealed no veins in the region approximately 1 μm from their side surfaces, possibly because a microstructure containing edge dislocations did not exist in this region owing to the image force from the surfaces. In contrast, 2- μm -wide specimens exhibited eminent extrusions and crack-like intrusions that were unexpected at low stress amplitudes. Veins did not develop within the specimens because the surface-affected regions occupied the entirety of the gauge part. Instead, a narrow dislocation wall emerged. The plastic deformation of this specimen was carried by screw dislocations on both sides of the wall. This structure and deformation mechanism resembled a ladder-like morphology of PSBs in the bulk metal. Results indicate that metal single crystals featuring dimensions on the order of a few micrometers can reach fatigue failure even under low stress amplitudes, primarily due to the absence of vein formations, elucidating a critical aspect of fatigue behavior in small-scale metals.

CRedit authorship contribution statement

Takashi Sumigawa: Conceptualization, Data curation, Funding acquisition, Investigation, Methodology, Project administration, Supervision, Validation, Visualization, Writing – original draft, Writing – review & editing. **Nobutaka Kawakatsu:** Data curation, Investigation, Visualization, Validation. **Akihiro Tobise:** Data curation, Investigation, Visualization, Validation. **Kota Sugisaka:** Data curation, Investigation, Visualization, Validation. **Yoshimasa Takahashi:** Investigation, Visualization. **Shigeo Arai:** Investigation, Visualization. **Masataka Abe:** Writing – review & editing, Investigation. **Hiroyuki Shima:** Writing – review & editing, Supervision. **Yoshitaka Umeno:** Writing – review & editing, Supervision.

Declaration of competing interest

The authors have no competing interests to disclose.

Acknowledgment

This work was supported by JST CREST grant no. JPMJCR2092 and by JSPS KAKENHI grant nos. JP20K20963, JP22K18754, and JP 24H00283. The Nagoya University Microstructural Characterization Platform supported a part of this work as a program under the Nanotechnology Platform funded by the Ministry of Education, Culture, Sports, Science and Technology (MEXT), Japan.

Appendix

g·*b* analysis

Reducing the number of excited spots and extracting diffraction waves at a particular crystal plane is possible in TEM observations by shifting the incident direction of electron beam relative to the crystal zone axis. This feature can be used to analyze the characteristics of dislocations. When the following relation is established between the displacement vector of a dislocation, \mathbf{R} , and the diffraction vector, \mathbf{g} , the contrast of the dislocation disappears⁴⁴.

$$\mathbf{g} \cdot \mathbf{R} = 0, \quad (A.1)$$

where,

$$\mathbf{R} = A\mathbf{b} : \text{screw dislocation}, \quad \mathbf{R} = B\mathbf{b} + C(\mathbf{b} \times \mathbf{u}) : \text{edge dislocation}. \quad (A.2)$$

A, B, and C are constants, and \mathbf{u} is the unit vector in the dislocation line direction. Since the impact of the second term in the edge dislocation

equation is small, the disappearance condition for the dislocation is generally given by the following equation,

$$\mathbf{g} \cdot \mathbf{b} = 0. \quad (\text{A.3})$$

If two \mathbf{g} vectors (\mathbf{g}_1 and \mathbf{g}_2) are identified, satisfying the disappearance condition, the Burgers vector of the dislocation is determined by

$$\mathbf{b} = \mathbf{g}_1 \times \mathbf{g}_2. \quad (\text{A.4})$$

References

- Z.S. Basinski, A.S. Korbel, S.J. Basinski, The temperature dependence of the saturation stress and dislocation substructure in fatigued copper single crystals, *Acta Metall.* 28 (1980) 191–207, [https://doi.org/10.1016/0001-6160\(80\)90068-1](https://doi.org/10.1016/0001-6160(80)90068-1).
- A.T. Winter, O.R. Pedersen, K.V. Rasmussen, Dislocation microstructures in fatigued copper polycrystals, *Acta Metall.* 29 (1981) 735–748, [https://doi.org/10.1016/0001-6160\(81\)90117-6](https://doi.org/10.1016/0001-6160(81)90117-6).
- H. Mughrabi, Dislocation wall and cell structures and long-range internal stresses in deformed metal crystals, *Acta Metall.* 31 (1983) 1367–1379, [https://doi.org/10.1016/0001-6160\(83\)90007-X](https://doi.org/10.1016/0001-6160(83)90007-X).
- C. Laird, P. Charsley, H. Mughrabi, Low energy dislocation structures produced by cyclic deformation, *Mater. Sci. Eng.* 81 (1986) 433–450, [https://doi.org/10.1016/0025-5416\(86\)90281-8](https://doi.org/10.1016/0025-5416(86)90281-8).
- S.J. Basinski, Z.S. Basinski, A. Howie, Early stages of fatigue in copper single crystals, *Philos. Mag.* 19 (1969) 899–924, <https://doi.org/10.1080/14786436908225856>.
- H. Mughrabi, The cyclic hardening and saturation behaviour of copper single crystals, *Mater. Sci. Eng.* 33 (1978) 207–223, [https://doi.org/10.1016/0025-5416\(78\)90174-X](https://doi.org/10.1016/0025-5416(78)90174-X).
- Z.S. Basinski, S.J. Basinski, Copper single crystal PSB morphology between 4.2 and 350K, *Acta Metall.* 37 (1989) 3263–3273, [https://doi.org/10.1016/0001-6160\(89\)90199-5](https://doi.org/10.1016/0001-6160(89)90199-5).
- P. Li, S.X. Li, Z.G. Wang, Z.F. Zhang, Fundamental factors on formation mechanism of dislocation arrangements in cyclically deformed fcc single crystals, *Prog. Mater. Sci.* 56 (2011) 328–377, <https://doi.org/10.1016/j.pmatsci.2010.12.001>.
- K. Mecke, C. Blochwitz, Saturation dislocation structures in cyclically deformed nickel single crystals of different orientations, *Cryst. Res. Technol.* 17 (1982) 743–758, <https://doi.org/10.1002/crat.2170170610>.
- J. Bretschneider, C. Holste, B. Tippelt, Cyclic plasticity of nickel single crystals at elevated temperatures, *Acta Mater.* 45 (1997) 3775–3783, [https://doi.org/10.1016/S1359-6454\(97\)00030-X](https://doi.org/10.1016/S1359-6454(97)00030-X).
- C. Buque, Dislocation structures and cyclic behaviour of [011] and [111]-oriented nickel single crystals, *Int. J. Fatigue* 23 (2001) 671–678, [https://doi.org/10.1016/S0142-1123\(01\)00032-9](https://doi.org/10.1016/S0142-1123(01)00032-9).
- H. Mughrabi, F. Ackermann, K. Herz, Fatigue mechanisms (J.T. Fong (Ed.)), *ASTM Spec Tech Publ* 675 (1979), 69–94.
- Y. Kaneko, Y. Morita, S. Hashimoto, Change in shape of hysteresis loop during cyclic deformation on austenitic stainless steel single crystals oriented for single slip, *Scr. Mater.* 37 (1997) 963–968, [https://doi.org/10.1016/S1359-6462\(97\)00150-4](https://doi.org/10.1016/S1359-6462(97)00150-4).
- N. Thompson, N. Wadsworth, N. Louat, The origin of fatigue fracture in copper, *Philos. Mag.* 1 (1956) 113–126, <https://doi.org/10.1080/14786435608238086>.
- E.E. Laufer, W.N. Roberts, Dislocations and persistent slip bands in fatigued copper, *Philos. Mag.* 14 (1966) 65–78, <https://doi.org/10.1080/14786436608218989>.
- A.T. Winter, Nucleation of persistent slip bands in cyclically deformed copper crystals, *Philos. Mag.* 37 (1978) 457–463, <https://doi.org/10.1080/14786436608218989>.
- J. Man, K. Obrtlík, J. Polák, Extrusions and intrusions in fatigued metals. Part I. State of the art and history, *Philos. Mag.* 89 (2009) 1295–1336, <https://doi.org/10.1080/14786430902917616>.
- H. Mughrabi, Microscopic mechanisms of metal fatigue, in: *Proceedings of the 5th International Conference on the Strength of Metals and Alloys*, 1979, pp. 1615–1638, <https://doi.org/10.1016/B978-1-4832-8412-5.50248-4>, 3, Pergamon, Oxford.
- J. Polák, J. Man, T. Vystavěl, M. Petreñec, The shape of extrusions and intrusions and initiation of stage I fatigue cracks, *Mater. Sci. Eng.* 517 (2009) 204–211, <https://doi.org/10.1016/j.msea.2009.03.070>.
- P.J.E. Forsyth, Exudation of material from slip bands at the surface of fatigued crystals of an aluminium-copper alloy, *Nature* 171 (1953) 172–173, <https://doi.org/10.1038/171172a0>.
- M.A. Bao-Tong, C. Laird, Overview of fatigue behavior in copper single crystals—I. Surface morphology and stage I crack initiation sites for tests at constant strain amplitude, *Acta Metall.* 37 (1989) 325–336, [https://doi.org/10.1016/0001-6160\(89\)90217-4](https://doi.org/10.1016/0001-6160(89)90217-4).
- Z.S. Basinski, S.J. Basinski, Fundamental aspects of low amplitude cyclic deformation in face-centred cubic crystals, *Prog. Mater. Sci.* 36 (1992) 89–148, [https://doi.org/10.1016/0079-6425\(92\)90006-S](https://doi.org/10.1016/0079-6425(92)90006-S).
- J.M. Finney, C. Laird, Strain localization in cyclic deformation of copper single crystals, *Philos. Mag.* 31 (1975) 339–366, <https://doi.org/10.1080/14786437508228937>.
- E. Demir, D. Raabe, Mechanical and microstructural single-crystal Bauschinger effects: observation of reversible plasticity in copper during bending, *Acta Mater.* 58 (2010) 6055–6063, <https://doi.org/10.1016/j.actamat.2010.07.023>.
- D. Kiener, C. Motz, W. Grosinger, D. Weygand, R. Pippan, Cyclic response of copper single crystal micro-beams, *Scr. Mater.* 63 (2010) 500–503, <https://doi.org/10.1016/j.scriptamat.2010.05.014>.
- T. Sumigawa, R. Shiohara, K. Matsumoto, T. Kitamura, Characteristic features of slip bands in submicron single-crystal gold component produced by fatigue, *Acta Mater.* 61 (2013) 2692–2700, <https://doi.org/10.1016/j.actamat.2013.01.053>.
- H. Fang, R. Shiohara, T. Sumigawa, T. Kitamura, Size dependence of fatigue damage in sub-micrometer single crystal gold, *Mater. Sci. Eng. A* 618 (2014) 416–423, <https://doi.org/10.1016/j.msea.2014.09.017>.
- K. Huang, T. Sumigawa, T. Kitamura, Experimental evaluation of loading mode effect on plasticity of microscale single-crystal copper, *Mater. Sci. Eng. A* 806 (2021) 140822, <https://doi.org/10.1016/j.msea.2021.140822>.
- T. Sumigawa, B. Kim, Y. Mizuno, T. Morimura, T. Kitamura, *In situ* observation on formation process of nanoscale cracking during tension-compression fatigue of single crystal copper micron-scale specimen, *Acta Mater.* 153 (2018) 270–278, <https://doi.org/10.1016/j.actamat.2018.04.061>.
- T. Sumigawa, S. Uegaki, T. Yukishita, S. Arai, Y. Takahashi, T. Kitamura, FE-SEM *in situ* observation of damage evolution in tension-compression fatigue of micro-sized single-crystal copper, *Mater. Sci. Eng. A* 764 (2019) 138218, <https://doi.org/10.1016/j.msea.2019.138218>.
- S. Lavenstein, Y. Gu, D. Madiseti, J.A. El-Awady, The heterogeneity of persistent slip band nucleation and evolution in metals at the micrometer scale, *Science* 370 (2020) eabb2690, <https://doi.org/10.1126/science.abb2690>.
- K. Huang, T. Sumigawa, T. Kitamura, Load-dependency of damage process in tension-compression fatigue of microscale single-crystal copper, *Int. J. Fatigue* 133 (2020) 105415, <https://doi.org/10.1016/j.ijfatigue.2019.105415>.
- R.K. Ham, The determination of dislocation densities in thin film, *Philos. Mag.* 6 (1961) 1183–1184, <https://doi.org/10.1080/14786436108239679>.
- R.B. Heywood, *Designing Against Fatigue*, Chapman and Hall, London, 1962.
- H. Shima, Y. Umeno, T. Sumigawa, Analytic formulation of elastic field around edge dislocation adjacent to slanted free surface, *R. Soc. Open Sci.* 9 (2022) 220151, <https://doi.org/10.1098/rsos.220151>.
- A. Tobise, H. Shima, Y. Akiba, Y. Umeno, E. Kawai, A. Kubo, M. Abe, T. Sumigawa, Surface outflow effect on dislocation structures in micrometer-sized metals, *Extrem. Mech. Lett.* 65 (2023) 102094, <https://doi.org/10.1016/j.eml.2023.102094>.
- C. Dan, Y. Cui, Y. Wu, Z. Chen, H. Liu, G. Ji, Y. Xiao, H. Chen, M. Wang, J. Liu, L. Wang, Y. Li, A. Addad, Y. Zhou, S. Ma, Q. Shi, H. Wang, J. Lu, Achieving ultrahigh fatigue resistance in AlSi10Mg alloy by additive manufacturing, *Nat. Mater.* 22 (2023) 1182–1188, <https://doi.org/10.1038/s41563-023-01651-9>.